Nanoscale Research Letters
a SpringerOpen Journal

NANO EXPRESS Open Access

Carboxymethyl chitosan-folic acid-conjugated Fe_3O_4@SiO_2 as a safe and targeting antitumor nanovehicle *in vitro*

Hongmei Li[1,2], Zhen Li[2], Jin Zhao[2], Baoqiang Tang[2], Yanhong Chen[2], Yikun Hu[2], Zhengda He[2] and Yue Wang[1,2*]

Abstract

A synthetic method to prepare a core-shell-structured Fe_3O_4@SiO_2 as a safe nanovehicle for tumor cell targeting has been developed. Superparamagnetic iron oxide is encapsulated inside nonporous silica as the core to provide magnetic targeting. Carboxymethyl chitosan-folic acid (OCMCS-FA) synthesized through coupling folic acid (FA) with OCMCS is then covalently linked to the silica shell and renders new and improved functions because of the original biocompatible properties of OCMCS and the targeting efficacy of FA. Cellular uptake of the nanovehicle was assayed by confocal laser scanning microscope using rhodamine B (RB) as a fluorescent marker in HeLa cells. The results show that the surface modification of the core-shell silica nanovehicle with OCMCS-FA enhances the internalization of nanovehicle to HeLa cells which over-express the folate receptor. The cell viability assay demonstrated that Fe_3O_4@SiO_2-OCMCS-FA nanovehicle has low toxicity and can be used as an eligible candidate for drug delivery system. These unique advantages make the prepared core-shell nanovehicle promising for cancer-specific targeting and therapy.

Keywords: Iron oxide; Surface functionalization; Tumor target; Surface modification

Background

Recently, considerable effort has been devoted to magnetic nanoparticles (NPs) as novel nanovehicles [1] and targeting agents [2] for biological and biomedical applications [3,4]. Iron oxide (Fe_3O_4) has emerged as one of the appealing candidates for drug delivery system [5] and magnetic fluorescence imaging [6,7]. However, the aggregations of naked Fe_3O_4 NPs decrease their interfacial areas, thus resulting in the loss of magnetism [8] and dispersibility [9]. Therefore, extensive work has been done to stabilize the NPs [10,11]. Huang synthesized uniform Fe_3O_4@SiO_2 NPs with well-controlled shell thickness [12]. Kaskel developed a homogeneous Fe_3O_4@SiO_2 with hollow mesoporous structure for drug delivery [13]. Unfortunately, the common challenge among these applications is to ensure sufficient uptake of NPs by specific cells [14,15]. The outer shell of silica not only protects the inner magnetite core from aggregation [16,17] but also provides sites for flexible surface modification such as poly(ethylene glycol) to render NP biocompatibility by preventing the nonspecific adsorption of proteins [18] and various targeting biomolecules [19,20] to improve the targeting efficiency. Kim reported Fe_3O_4@SiO_2 NPs using CTAB as a template and PEG to prolong the short blood half-life of NPs [21]. However, the safety of drug carriers is one of the most critical factors to ensure its efficacy. Carboxymethyl chitosan (OCMCS) is a water-soluble chitosan which receives a great deal of interest because of favorable biocompatibility, safety, nonimmunogenicity, as well as reasonable cost [22]. Shi reported the OCMCS-Fe_3O_4 easily internalized into cells via endocytosis [23]. Fan developed the Fe_3O_4 NPs with OCMCS which significantly reduced the cytotoxicity and the capture of NPs. Moreover, folic acid (FA)-modified OCMCS-Fe_3O_4 NPs combined receptor-mediated targeting and magnetic targeting together [24]. It is noted that folic acid, as an effective target ligand [25,26], shows high binding affinity with folate receptor, which over-expressed on the membranes of many human malignant cells, but limited on the normal

* Correspondence: zwy_1115@126.com
[1]State Key Laboratory of Coordination Chemistry, School of Chemistry and Chemical Engineering, Nanjing University, Nanjing 210008, China
[2]State Key Laboratory of Natural Medicines, School of Sciences, China Pharmaceutical University, Nanjing 211198, China

cells. To the best of our knowledge, the general synthetic protocols to combine silica with diverse functional modification used as a safe drug delivery system are seldom reported. With regard to the above effects, we develop a novel carboxymethyl chitosan-based, silica-coated iron oxide nanovehicle (Fe_3O_4@SiO_2-OCMCS-FA) with dual-targeting function (magnetic/folate) in this study. Fe_3O_4 core serves as a carrier for magnetic targeting, while silica coating on the iron oxide NPs offers sites for further modifications. OCMCS-FA was conjugated firstly to perform a folate receptor (FR)-mediated cellular endocytose and acted as the biocompatible segment and then subsequently coupled through acylation to the surface of animated Fe_3O_4@SiO_2 which was modified with (3-aminopropyl) triethoxysilane (APTES) to obtain the multifunctional nanovehicle (Fe_3O_4@SiO_2-OCMCS-FA). Its uptake by human cervical carcinoma cell lines (HeLa cells) is traced, and the cytotoxicity on the human tumor cells and normal cells are both evaluated. The results show that it is nontoxic to them, which reveal that it could be used as a promising candidate for drug target delivery system.

Methods

Reagent materials

All chemicals are analytical reagent grade and were used as received. Folic acid is a biological reagent purchased from Sinopharm Chemical Reagent Co., Ltd., Shanghai, China.

Synthesis of magnetic Fe_3O_4@SiO_2 NPs

Monodispersed Fe_3O_4 NPs were prepared by the thermal decomposition of ferric acetylacetonate precursor in the presence of an oleic acid stabilizer and oleylamine [27]. SiO_2 coating on the Fe_3O_4 NPs was performed through the formation of water-in-cyclohexane reverse microemulsion [28] (Figure 1).

Polyoxyethylene(5) nonylphenyl ether (5 mL, Igepal CO-520, Sigma-Aldrich, St. Louis, MO, USA) was firstly dispersed in cyclohexane (40 mL). Then, 2 mL Fe_3O_4 solution (50 mg mL^{-1} in cyclohexane) was added. After 10 min, ammonium hydroxide (292 μL) was added to form a transparent brown solution of reverse microemulsion. Next, tetraethylorthosilicate (TEOS) was added and the reaction was continued at room temperature for 24 h. When isopropanol was added into the reaction solution, Fe_3O_4@SiO_2 NPs were precipitated. They were collected by centrifugation and washed with ethanol. Fe_3O_4@SiO_2 NPs were then dried in vacuum at 60°C.

Synthesis of OCMCS-FA conjugate

The synthesis of OCMCS-FA conjugate was adopted by homogeneous synthesis through acylation (Figure 2). Folic acid (0.884 g) was dissolved in 20 mL of anhydrous dimethylsulfoxide (DMSO) to which dicyclohexylcarbodiimide (DCC; 0.784 g) and *N*-hydroxysuccinimide (NHS; 0.256 g) were added. The reaction mixture was stirred for 24 h at 45°C in the dark [29]. The by-product dicyclohexylurea was filtered off, and 20 mL of 30% acetone in diethyl ether was added with stirring. A yellow precipitate (NHS-FA) formed and was collected after washing with diethyl ether several times. Then, 100 mg OCMCS was dissolved in acetate buffer (pH 4.7). A mixture solution of NHS-FA and 1-ethyl-3-(3-dimethylaminopropyl) carbodiimide (EDC) was prepared by dissolving NHS-FA and EDC simultaneously in DMSO. Finally, the mixture solution was dropped into the OCMCS solution. After 24 h, the solution was adjusted to pH 9 with NaOH and purified by centrifugation followed by 2 days of dialysis against phosphate-buffered solution (PBS) and extensive dialysis against water using a 3,500-Da cutoff dialysis membrane. OCMCS-FA was then dried in vacuum at 60°C.

Synthesis of Fe_3O_4@SiO_2-OCMCS-FA NPs

APTES was anchored to the surface of Fe_3O_4@SiO_2 through refluxing at 110°C in toluene to develop amide in the surface of silica in order to introduce carboxyl groups of OCMCS-FA conjugate. Fifty milligrams of APTES-modified Fe_3O_4 was added to 10 mL of a 2-(*N*-morpholino) ethanesulfonic acid buffer (0.1 M, pH 6.5) containing 50 mg of OCMCS-FA, EDC (20 mM), and NHS (50 mM). The mixture suspension was then sonicated for 10 min in ultrasonic disrupter and shaken for 24 h at room temperature. The OCMCS-FA bound Fe_3O_4@SiO_2 were collected under centrifugation, washed with ethanol, and dried in vacuum at 60°C.

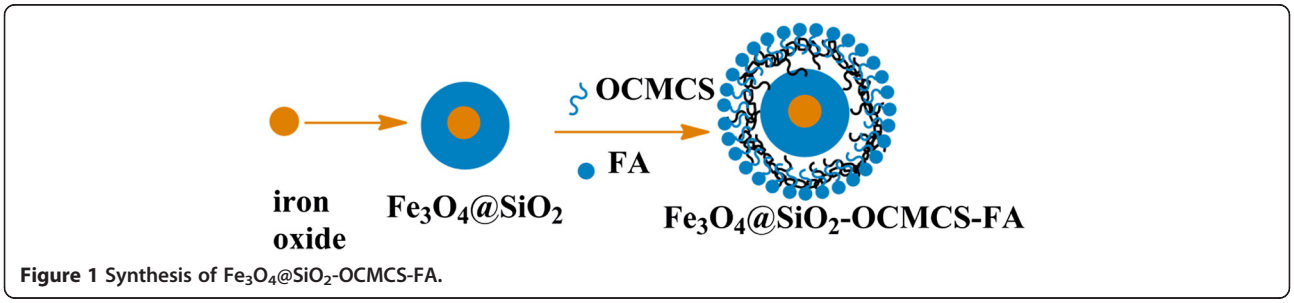

Figure 1 Synthesis of Fe_3O_4@SiO_2-OCMCS-FA.

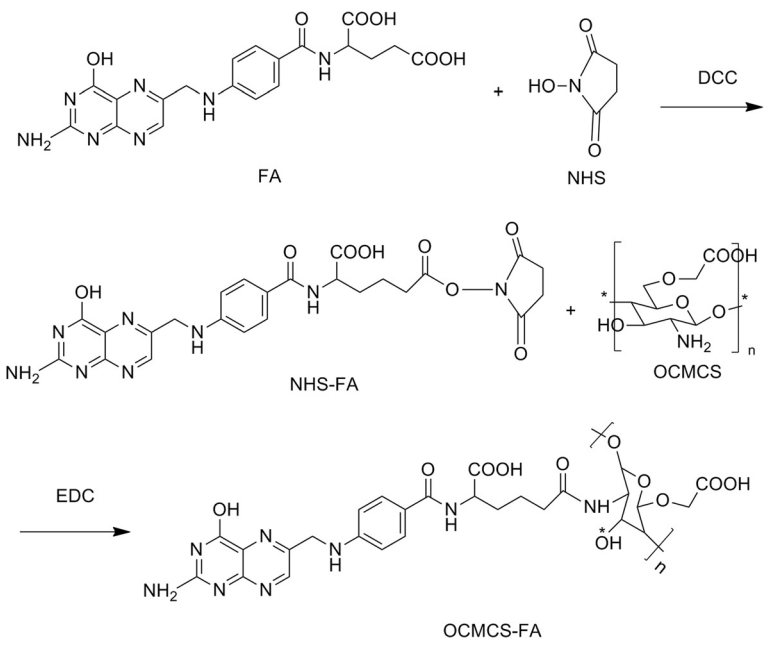

Figure 2 Synthesis of OCMCS-FA.

Hemolysis assay

Two milliliters of rat blood was injected from the eye socket vein. The red blood cells (RBCs) were obtained by removing the serum from the blood by centrifugation and suction. After being washed with PBS solution five times, the RBCs were diluted to 1/10 of their volume with PBS solution. Diluted RBC suspension (0.3 mL) was then mixed with the following: (a) PBS (1.2 mL) as a negative control, (b) deionized water (1.2 mL) as a positive control, and (c) nanovehicle suspensions (1.2 mL) at concentrations ranging from 40 to 500 μg mL^{-1}. The mixtures were then vortexed and kept for 2 h at room temperature. Finally, the mixtures were centrifuged for 2 min at 4,000 rpm and the absorbance of the upper supernatants at 541 nm was measured by UV-visible (UV-vis) characterization. The percentage of hemolysis was calculated using the following equation (A is the absorbance of UV-vis spectra) [30]:

$$\text{Hemolysis} = \left(A_{\text{sample}} - A_{(-)\text{control}}\right) / \left(A_{(+)\text{control}} - A_{(-)\text{control}}\right)$$

Cell culture and uptake

HeLa cell lines were maintained in Dulbecco's modified Eagle's medium (DMEM) containing 10% fetal bovine serum, 100 units mL^{-1} penicillin, and 100 mg mL^{-1} streptomycin in 37°C, 5% CO_2. For investigation on targeting of nanovehicles, nanovehicles were labeled with RB to form $RBFe_3O_4@SiO_2$ and $RBFe_3O_4@SiO_2$-OCMCS-FA nanoparticles [31]. In a typical procedure, 2.5×10^4 cells were seeded in a 35-mm dish with a glass bottom for 24 h to allow the cells to attach. After the cells were washed twice with PBS, the samples were added to the dishes in a concentration of 100 μg mL^{-1}. After 2 h of incubation, the cells were washed several times with PBS to remove the remaining samples and dead cells. Finally, the cells were observed under a confocal laser scanning microscope (CLSM; Carl Zeiss LSM 710, Oberkochen, Germany). Cells with the addition of $Fe_3O_4@SiO_2$ were imaged as control.

Bio-TEM observations for HeLa cells

The HeLa cells were incubated with 2.5 μg mL^{-1} nanovehicle inDMEM in 5% CO_2 at 37°C for 24 h. Afterwards, cells were washed three times with PBS and subsequently fixed with 2.5% glutaraldehyde in 0.03 M potassium phosphate buffer for at least 24 h. Cells were then washed in PBS, postfixed with 1% osmium tetroxide in sodium carboxylate buffer, washed with 0.05 mol L^{-1} maleate, and stained with 0.5% uranylacetate (Sigma-Aldrich) in maleate buffer. After washing the cells in 0.05 mol L^{-1} maleate, the cells were dehydrated in a grading series of ethanol followed by acetone, embedded in Epon (Momentive Specialty Chemicals, Inc., Columbus, OH, USA), and dried in an oven at 60°C for 4 days. Ultrathin sections of approximately 50 nm thick were cut with a diamond knife on a Leica Ultracut R ultramicrotome (Milton Keynes, UK) and transferred to the copper grid. The images were viewed on JEOL-2100 electron microscope (Akishima, Tokyo, Japan).

Cytotoxicity

The *in vitro* cytotoxicity was measured by using the 3-(4,5-dimethylthiazol-2-yl)-2,5-diphenyltetrazolium bromide (MTT) assay in HeLa cells. Cells were initially seeded into a 96-well cell culture plate at 1×10^4 per well and then incubated for 24 h at 37°C under 5% CO_2. DEME solutions of nanovehicle at concentrations of 100 mg mL^{-1} were added to the wells. The cells were further incubated for 72 h at 37°C under 5% CO_2. The cells were washed three times with 0.2 mL PBS to remove the unbound nanoparticles. Subsequently, 0.2 mL DEME and 25 mL MTT (5 mg mL^{-1}) were added to each well and incubated for an additional 4 h at 37°C under 5% CO_2. Then, the medium solution was replaced by 0.15 mL DMSO solution. After 10 min, the optical density at 490 nm (absorption value) of each well was measured on a Tecan Infinite M 200 monochromator-based multifunction microplate reader (Männedorf, Switzerland). The corresponding nanovehicle with cells but not treated by MTT were used as controls. The cell vitality after labeling was compared with that of unlabeled cells and expressed as the relative ratio.

Characterization

^{1}H NMR spectra was recorded at 300 MHz on a Bruker ARX 300 spectrometer (Ettlingen, Germany). Infrared spectra (4,000 to 400 cm^{-1}) were recorded on Bruker Fourier transform infrared (FTIR) spectrometer in KBr pellets. The X-ray powder diffraction patterns were recorded on an X'Pert diffractometer (PANalytical B.V., Almelo, The Netherlands) with CuKα radiation (λ = 1.54060 Å) at 45 kV and 40 mA. X-ray photoelectron spectroscopy (XPS) analysis was performed with a ESCALB MK-II (Physical Electronics Instruments, Chanhassen, MN, USA). The source was the monochromatic MgKα radiation. The surface charge of the nanovehicles was investigated on Malvern Zetasizer Nano ZS 90 zeta potential analyzer (Westborough, MA, USA). Transmission electron microscopy (TEM) was performed on a JEOL-2100 with an accelerating voltage of 200 kV. TEM samples were prepared by drop-casting dispersion onto copper grids covered by carbon film. Ultrathin sections for bio-TEM were cut with a diamond knife on a Leica Ultracut R ultramicrotome. Scanning electron microscopy (SEM) was performed on a JEOL-S-3400 N II. Magnetic property measurements were performed using a Quantum Design MPMS XL-7 superconducting quantum interference device (SQUID; Olomouc, Czech Republic). Confocal images were acquired using a Zeiss confocal laser scanning unit mounted on an LSM 710 fixed-stage upright microscope.

Results and discussion

The ^{1}H NMR spectra of OCMCS-FA conjugate was shown in Figure 3. The signals at δ 1.65, 2.88, and 3.08 to 3.64 ppm was assigned to the resonance of the monosaccharide residue protons, -$COCH_3$, -CH-NH-, and -CH_2-O-, respectively. The signals appearing at δ 6.3 to 8.5 ppm were attributed to the resonance of the folate aromatic protons. So, it revealed that the couple of the FA residue to the OCMCS could be achieved via EDC mediation [32].

FTIR spectroscopy shown in Figure 4 confirmed that OCMCS-FA was successfully immobilized on the Fe_3O_4@SiO_2 NPs. In the spectrum of OCMCS-FA (Figure 4b), the 1,635 cm^{-1} peak of COO- stretching vibration shifted to 1,590 cm^{-1} compared to OCMCS (Figure 4a). Moreover, a shoulder peak around 1,710 cm^{-1}

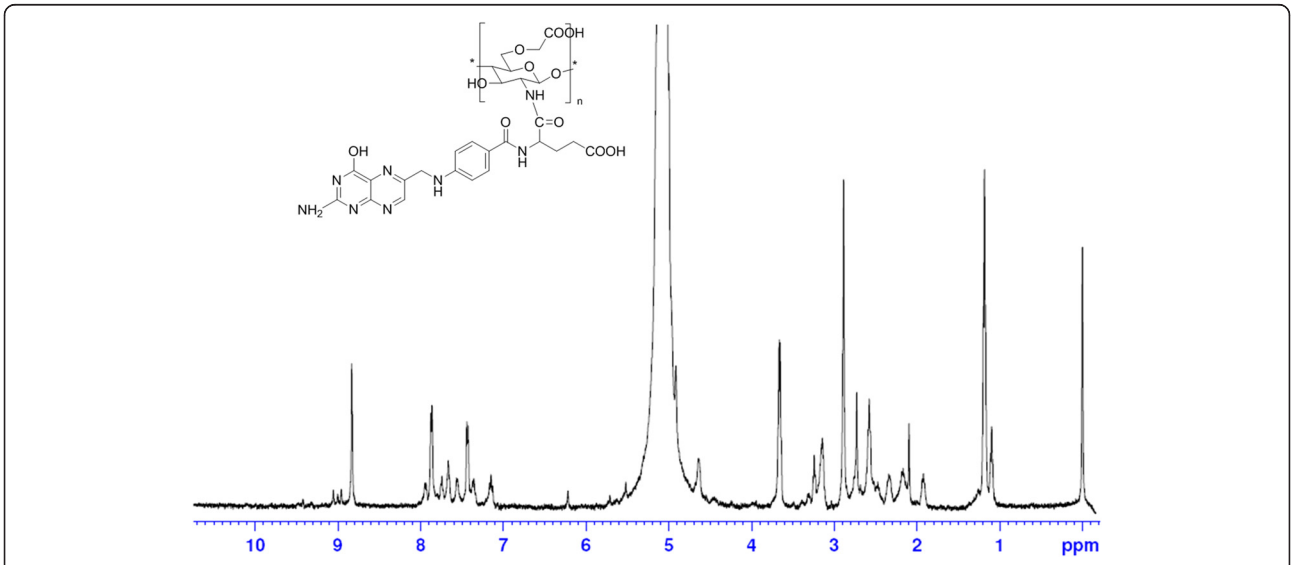

Figure 3 ^{1}H NMR spectra of OCMCS-FA in CF_3COOD/D_2O.

is observed in OCMCS-FA which verified that FA conjugated to the OCMCS successfully [33]. The bare Fe_3O_4 NPs showed characteristic bands related to the Fe-O vibrations near 569 cm^{-1} (Figure 4b,c). The peak at 1,100 cm^{-1} indicated Si-O bonding on the NP surface (Figure 4c). Unsurprisingly, the FTIR spectra for Fe_3O_4@-SiO_2-OCMCS-FA nanovehicle presented similar peaks at 1,710, 1,590, 1,100, and 569 cm^{-1} (Figure 4d). What is more, the FTIR spectrum of Fe_3O_4@SiO_2-OCMCS-FA nanovehicle displayed an intense peak at 1,650 cm^{-1} which might result from the -CONH- due to the reaction between the carboxyl group of the OCMCS and amide on the surface of silica.

The XRD measurements were performed with the dried powder samples of bare, silica-coated and OCMCS-FA-conjugated iron oxide to identify the crystal phases. The pattern of OCMCS-FA-conjugated NPs (Figure 5) showed all the major peaks corresponding to Fe_3O_4 which could be assigned to the (311), (511), and (440) planes, respectively [34]. Additionally, the peak around $2\theta = 25°$ due to the silica [35] was observed in the case of the silica-coated NPs, but disappeared in the Fe_3O_4@SiO_2-OCMCS-FA nanovehicle which may attribute to the OCMCS-FA conjugated. These results confirmed the surface modification of the Fe_3O_4 NPs with OCMCS-FA.

The surface composition was also ascertained by XPS as it is recognized as a quantitative surface elemental analysis and chemical state information. Wide-scan spectra were acquired for NPs with high-resolution C 1s, O 1s, and N 1s. Spectral calibration was carried out by setting the main C 1s peak at 285 eV. The high-resolution scans for C 1s (Figure 6a) of Fe_3O_4@SiO_2-OCMCS-FA nanovehicle could be deconvoluted into four peaks at 285.7, 284.5, 286.3, and 288.2 eV, which could be attributed to -C-O-, -C-C-, -NH-C = O, and -COOH groups, respectively. The O 1 s spectrum (Figure 6b) of nanovehicle displayed three peaks at 532.3, 532.6, and 530.9 eV corresponding to oxygen being present in three different environments as -C-O, -O-H, and C = O in Fe_3O_4@SiO_2-OCMCS-FA nanovehicle. Compared with the free folate, OCMCS-FA, and Fe_3O_4@SiO_2-OCMCS-FA, distinction was made towards the high-resolution scans for N 1s. Free folate (Figure 6e) could be deconvoluted into four peaks at 399. 9, 400.1, 399.5, and 398.5 eV. The bands at 398.5 and 399.5 eV are due to the amide N and other N of FA, respectively. The bands at 400.1 and 399.9 eV were in accordance with those of triazole ring N as reported [36]. However, the peak of free amide N at 398.5 eV disappeared in the spectrum of OCMCS-FA (Figure 6d), and a new peak at 400.8 eV appeared due to the amide conjugation between FA and OCMCS. Interestingly, the N 1-s spectrum of Fe_3O_4@SiO_2-OCMCS-FA nanovehicle (Figure 6c) showed similar peaks with OCMCS-FA except at 401.2 eV. The peak at 401.2 eV might be originated from the formation of amide linkage between the carboxyl group of the OCMCS and amide on the surface of silica which was reasonably consistent with the peak reported in the literature. Anyway, XPS results support OCMCS-FA chemically bound to the surface of Fe_3O_4@SiO_2 by amidation.

Moreover, the zeta potential of suspension for Fe_3O_4@SiO_2-OCMCS-FA was -28.89 ± 0.43 mV which was smaller than that of Fe_3O_4 NPs considering that

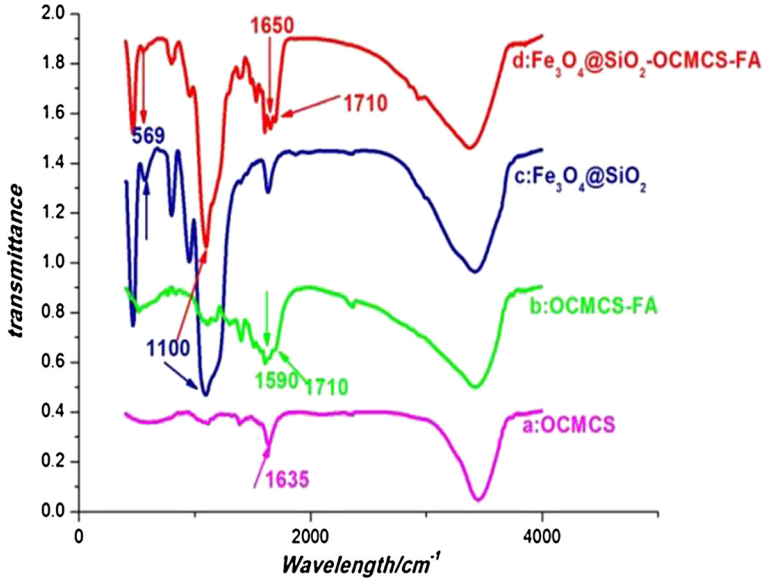

Figure 4 FTIR spectra. (a) OCMCS, **(b)** OCMCS-FA, **(c)** Fe_3O_4@SiO_2, and **(d)** Fe_3O_4@SiO_2-OCMCS-FA.

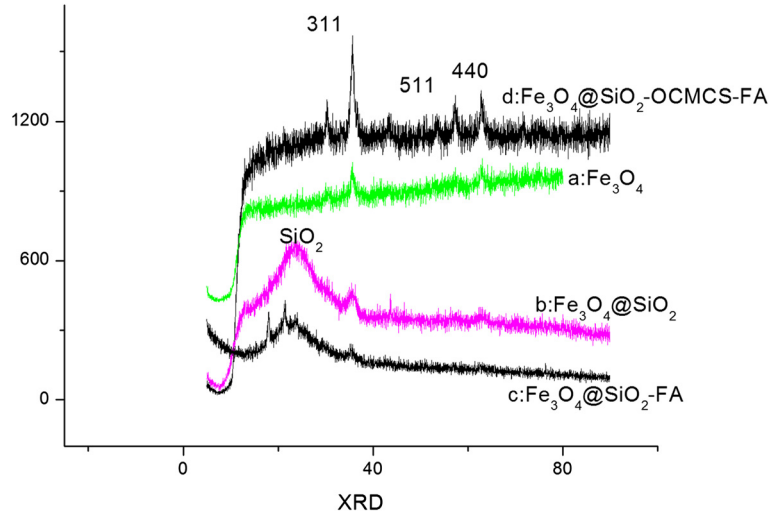

Figure 5 XRD spectrum. (a) Fe_3O_4 NPs, **(b)** Fe_3O_4@SiO_2, **(c)** Fe_3O_4@SiO_2-FA, and **(d)** Fe_3O_4@SiO_2-OCMCS-FA.

silica and OCMCS-FA modification protect the Fe_3O_4 NPs away from aggregation. As shown in Figure 7, spherical Fe_3O_4 NPs were chosen as the template to obtain multifunctional nanovehicle. It can be seen that spherical Fe_3O_4 NPs were about 6 to 8 nm in size with high dispersibility (Figure 7a, inset). The corresponding high-resolution image (Figure 7a, inset) showed clear lattice fringes which corresponds to Fe_3O_4. A thick layer of dense silica was deposited onto the surface of Fe_3O_4 with a core thickness of 7 nm and shell thickness of 14 nm (Figure 7a) with uniform particle size and excellent morphology. Then, a thin layer of OCMCS-FA conjugated to the surface of Fe_3O_4@SiO_2 through amidation with the aid of

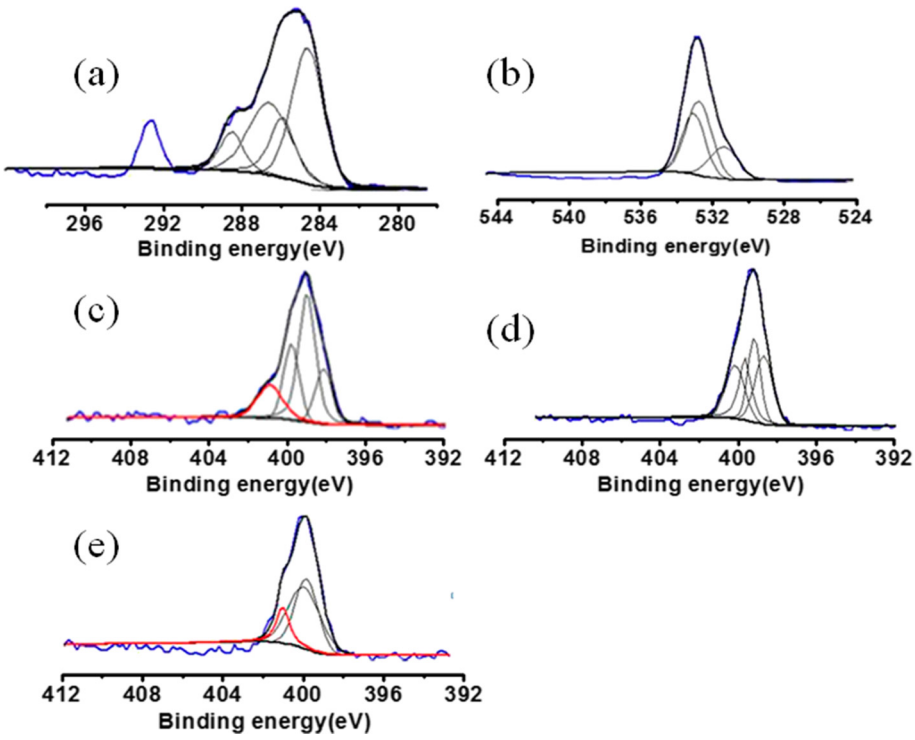

Figure 6 High-resolution C 1s, O 1s, and N 1s X-ray photoelectron spectra. (a) High-resolution C 1s spectrum of Fe_3O_4@SiO_2-OCMCS-FA, **(b)** high-resolution O 1s spectrum of Fe_3O_4@SiO_2-OCMCS-FA, **(c)** high-resolution N 1s spectrum of Fe_3O_4@SiO_2-OCMCS-FA, **(d)** high-resolution N 1s of OCMCS-FA, and **(e)** high-resolution N 1s spectrum of FA.

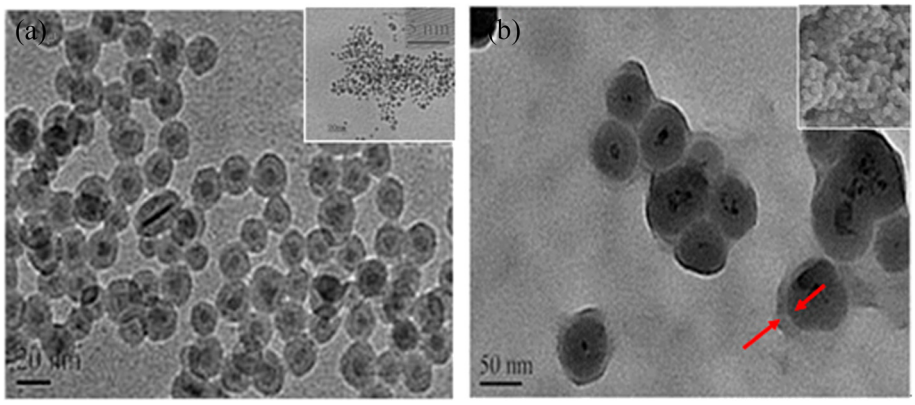

Figure 7 TEM images. (a) $Fe_3O_4@SiO_2$ (inset: Fe_3O_4) and **(b)** $Fe_3O_4@SiO_2$-OCMCS-FA (inset: SEM images of $Fe_3O_4@SiO_2$-OCMCS-FA).

sodium tripolyphosphate (TPP) forms a tri-layered (5 nm) multifunctional nanovehicle ($Fe_3O_4@SiO_2$-OCMCS-FA) (Figure 7b). The SEM image shows that the nanovehicles are very uniform in both size and shape (Figure 7b, inset).

The magnified hysteresis loop of $Fe_3O_4@SiO_2$-OCMCS-FA nanovehicle which clearly showed that no remanence and hysteresis were detected demonstrated the superparamagnetism of the nanovehicle (Figure 8). After coating with silica, the magnetization of $Fe_3O_4@SiO_2$ was undoubtedly decreased compared with the Fe_3O_4 nanoparticles for the shell and relatively low Fe_3O_4 amount. However, after the final modification of OCMCS-FA, the magnetization of the nanovesicles was not apparently decreased due to the thin outer layer. Factually, superparamagnetism is usually highly desired because it can prevent the magnetic composite particles from irreversible aggregation and ensure an excellent dispersibility once the applied magnetic field is removed [37].

In vitro targeting of nanovehicle

The ability of nanoparticles to target specific locations is one of the most important factors for their prospective application in drug delivery and biomedicine. To investigate the uptake possibility of $Fe_3O_4@SiO_2$-OCMCS-FA, CLSM was applied to trace the process of this nanovehicle. Therefore, RB is labeled on the surface of the nanovehicle to distinguish it. To explore the practical application of this nanovehicle in the targeting of tumor cells, the particles were incubated in physiological conditions with HeLa cells bearing the over-expressed folate receptor. Figure 9 shows DAPI, RB, and merged images of HeLa cells incubated with $RBFe_3O_4@SiO_2$ (20 μg mL^{-1}, control) and $RBFe_3O_4@SiO_2$-OCMCS-FA (20 μg mL^{-1}) for 2 h. Interestingly, even at the very low

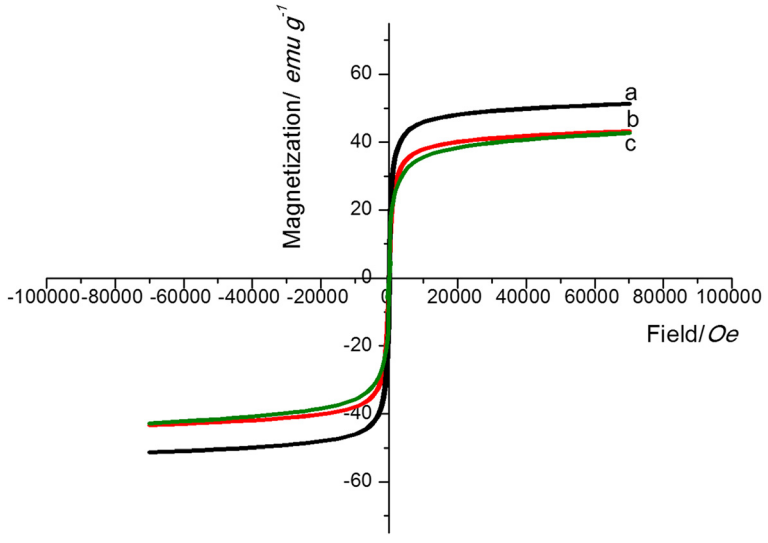

Figure 8 Magnetization curve. (a) Fe_3O_4 **(b)** $Fe_3O_4@SiO_2$, and **(c)** $Fe_3O_4@SiO_2$-OCMCS-FA nanovehicle at 300 K.

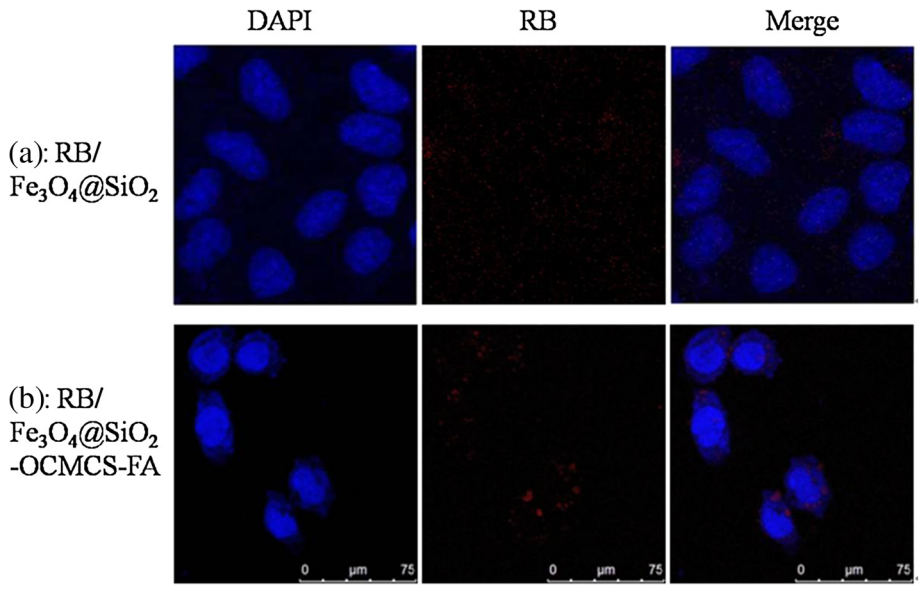

Figure 9 Confocal laser scanning microscope images of subcellular localization. (a) $RBFe_3O_4@SiO_2$ and **(b)** $RBFe_3O_4@SiO_2$-OCMCS-FA after 2 h of incubation with HeLa cells. Nuclei were stained with DAPI.

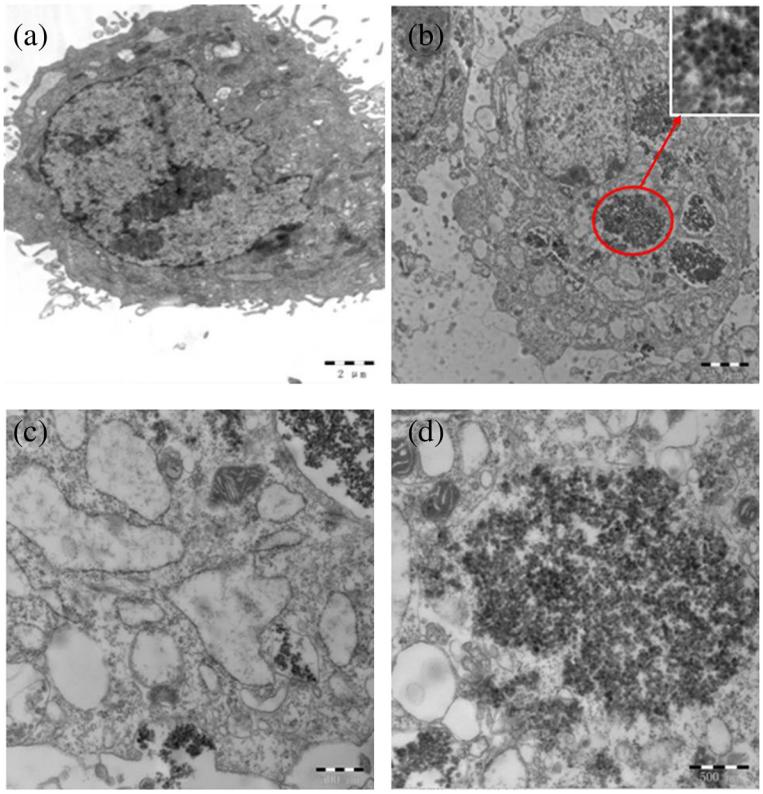

Figure 10 Bio-TEM images of HeLa cells after 24 h of exposure to NPs (100 μg mL^{-1}). (a) Control, **(b)** $Fe_3O_4@SiO_2$-OCMCS-FA nanovehicle (inset: magnified image of the circled area) and **(c, d)** magnified image of $Fe_3O_4@SiO_2$-OCMCS-FA nanovehicle.

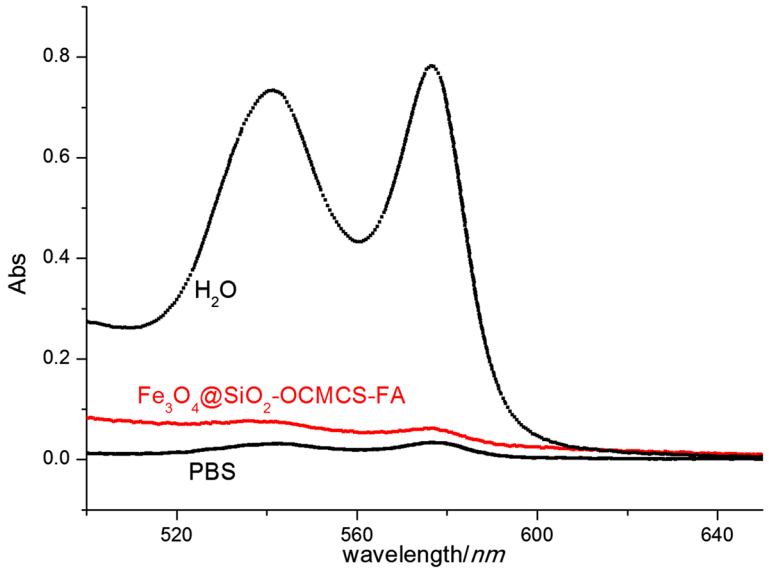

Figure 11 Percentage of hemolysis of RBCs in the presence of Fe_3O_4@SiO_2-OCMCS-FA at 500 μg mL^{-1}. Water (+) and PBS (–) are used as positive and negative controls, respectively.

concentration, the CLSM images show that the RBFe_3O_4@SiO_2-OCMCS-FA nanoparticles could be taken up by HeLa cells within a short period as manifested by the appearance of spot-like red fluorescence in cells (Figure 9b), while untreated RBFe_3O_4@SiO_2 showed negligible background fluorescence under similar imaging conditions (Figure 9a). The merge of the bright-field and fluorescent images further demonstrates that the luminescence is strongly correlated with the intracellular location (Figure 9b) suggesting the feasibility and efficiency of the nanoparticles for anticancer drug delivery into cancer cells. In addition, the fluorescent image shown in Figure 9b also testifies that the nanovehicle was mainly distributed in the cytoplasm after cellular uptake. The confocal laser scanning microscope observation confirms that the nanovehicle could be effectively taken up by the HeLa cells as the folate modified.

To further reveal that the nanovehicle was internalized in HeLa cells rather than being bound to the cell surface, bio-TEM was used to analyze the nanovehicle-treated cells. Unlike the untreated cells (Figure 10a), some aggregates of nanovehicles were observed as black patches inside the cell cytoplasm which maintained their core-shell structure (Figure 10b and the inset), while no nanovehicle was found in the nucleus which coincided with the results of CLSM. Based on the cell morphology, it is plausible that the nanovehicle accumulates on the membrane (Figure 10c) by the high specific interaction between folic acid on the nanovehicle and FR on HeLa cells which may increase the uptake through folate receptor-mediated endocytosis. Afterwards, majority of the internalized nanovehicle will be processed in lysosomes and are eventually released into the cytoplasm (Figure 10d). Therefore, *in vitro* CLSM and bio-TEM images present evidence about the target effects of nanovehicle with the OCMCS-FA modification.

Biocompatibility of nanovehicles (hemolysis assay and cytotoxicity)

It is important to investigate the biocompatibility of Fe_3O_4@SiO_2-OCMCS-FA nanovehicles when materials are administrated by vein injection. Hemolysis assay is a primary approach to assess the biocompatibility for *in vivo* applications. The hemolysis percentage of the nanovehicles was quantified based on the absorbance of the supernatant

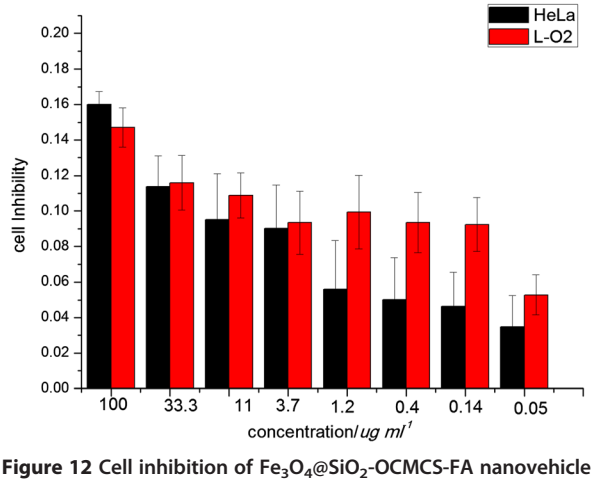

Figure 12 Cell inhibition of Fe_3O_4@SiO_2-OCMCS-FA nanovehicle on HeLa and L-O2 cells.

at 541 nm with isotonic PBS and distilled water as control. From Figure 11, Fe_3O_4@SiO_2-OCMCS-FA nanovehicle exhibits good biocompatibility, and the hemolysis percentage of Fe_3O_4@SiO_2-OCMCS-FA even at a high concentration of 500 μg mL^{-1} was 6.3% lower than the value of traditional nanoparticles (70% of 500 μg mL^{-1}) [38]. Thus, the obtained results showed that no visible hemolysis effect was observed visually for nanovehicle to evidence the good blood compatibility for the introduction of OCMCS.

In order to verify the toxicity of nanovehicle, *in vitro* cytotoxicity of the nanovehicle on HeLa and human liver cells (L-O2) was evaluated using a traditional MTT assay. The results (Figure 12) showed that there was a relatively high cell viability (more than 80% at a concentration of 100 μg mL^{-1}) in HeLa which displays low cytotoxicity and favorable cell compatibility which is consistent with hemolysis assay. In addition, the viability of the L-O2 cells was similar to that of the HeLa after incubating with nanovehicle which demonstrates that Fe_3O_4@SiO_2-OCMCS-FA possesses safety for normal cells as a drug carrier. The mesoporous silica layer of this nanovehicle is currently studied by our group, which may offer the platform for insoluble drugs in biomedical application.

Conclusions

In summary, we presented a rational method of preparing folic acid-conjugated carboxymethyl chitosan by homogeneous synthesis characterized by ^1H NMR and FTIR. Moreover, a novel, safe, and tumor-targeting nanovehicle with iron oxide as core and silica as shell has been fabricated showing good dispersion. It was firstly reported that OCMCS-FA conjugated on the surface of Fe_3O_4@SiO_2 via amide reaction to form the layer of compatibility and receptor-mediated targeting. Fe_3O_4@SiO_2-OCMCS-FA nanovehicle exhibits high uptake of HeLa cells which imply low cytotoxicity and good biocompatibility because of the dual targeting and OCMCS serving as a long circulation. Furthermore, the silica moiety of Fe_3O_4@SiO_2-OCMCS-FA nanovehicle could be extended to fabricate mesoporous nanovehicle which may increase surface area and pore volume. Thus, we believe that this strategy may provide a safe and efficient platform for antitumor drug delivery.

Competing interests

The authors declare that they have no competing interests.

Authors' contributions

HL and YW conceived and designed the experimental strategy and wrote the manuscript. JZ and YC prepared andperformed the synthetic experiments. YH analyzed the data. ZH and BT performed the *in vitro* experiments. ZL helped with the editing of the paper. All authors read and approved the final manuscript.

Acknowledgements

We gratefully acknowledge the assistance of Professor Zheng Xu from the State Key Laboratory of Coordination Chemistry in Nanjing University. The work was financially supported by the Fundamental Research Funds for the Central Universities (JKZD2013003).

Received: 22 January 2014 Accepted: 11 March 2014
Published: 25 March 2014

References

1. Shen JM, Yin T, Tian XZ, Gao FY, Xu S: **Surface charge-switchable polymeric magnetic nanoparticles for the controlled release of anticancer drug.** *ACS Appl Mater Interfaces* 2013, **5:**7014–7024.
2. Lee JH, Lee K, Moon SH, Lee YH, Park TG, Cheon J: **All-in-one target-cell-specific magnetic nanoparticles for simultaneous molecular imaging and siRNA delivery.** *Angew Chem Int Ed* 2009, **4:**4174–4179.
3. Lu AH, Salabas EL, Schüth F: **Magnetic nanoparticles: synthesis, protection, functionalization, and application.** *Angew Chem Int Ed* 2007, **46:**1222–1244.
4. Tassa C, Shaw SY, Weissleder R: **Dextran-coated iron oxide nanoparticles: a versatile platform for targeted molecular imaging, molecular diagnostics, and therapy.** *Acc Chem Res* 2011, **44:**842–852.
5. Thomas CR, Ferris DP, Lee JH, Choi E, Cho MH, Kim ES, Stoddart JF, Shin JS, Cheon J, Zink JI: **Noninvasive remote-controlled release of drug molecules in vitro using magnetic actuation of mechanized nanoparticles.** *J Am Chem Soc* 2010, **132:**10623–10625.
6. Yong KT, Roy I, Swihart MT, Prasad PN: **Multifunctional nanoparticles as biocompatible targeted probes for human cancer diagnosis and therapy.** *J Mater Chem* 2009, **19:**4655–4672.
7. Kim E, Lee K, Huh YM, Haam S: **Magnetic nanocomplexes and the physiological challenges associated with their use for cancer imaging and therapy.** *J Mater Chem B* 2013, **1:**729–739.
8. Hui C, Shen CM, Tian JF, Bao LH, Ding H, Li C, Tian Y, Shi XZ, Gao HJ: **Core-shell Fe_3O_4@SiO_2 nanoparticles synthesized with well-dispersed hydrophilic Fe_3O_4 seeds.** *Nanoscale* 2011, **3:**701–705.
9. Safi M, Courtois J, Seigneuret M, Conjeaud H, Berret JF: **The effects of aggregation and protein corona on the cellular internalization of iron oxide nanoparticle.** *Biomaterials* 2011, **32:**9353–9363.
10. Ling DS, Hyeon T: **Chemical design of biocompatible iron oxide nanoparticles for medical applications.** *Small* 2013, **9:**1450–1466.
11. Na HB, Palui G, Rosenberg JT, Ji X, Grant SC, Mattoussi H: **Multidentate catechol-based polyethylene glycol oligomers provide enhanced stability and biocompatibility to iron oxide nanoparticles.** *ACS Nano* 2012, **6:**389–399.
12. Huang CC, Tsai CY, Sheu HS, Chuang KY, Su CH, Jeng U, Cheng FY, Su CH, Lei HY, Yeh CS: **Enhancing transversal relaxation for magnetite nanoparticles in MR imaging using Gd^{3+}-chelated mesoporous silica shells.** *ACS Nano* 2011, **5:**3905–3916.
13. Zhu YF, Kockrick E, Ikoma T, Hanagata N, Kaskel S: **An efficient route to rattle-type Fe_3O_4@SiO_2 hollow mesoporous spheres using colloidal carbon spheres templates.** *Chem Mater* 2009, **21:**2547–2553.
14. Neoh KG, Kang ET: **Surface modification of magnetic nanoparticles for stem cell labeling.** *Soft Matter* 2012, **8:**2057–2069.
15. Dandamudi S, Patil V, Fowle W, Khaw BA, Campbell RB: **External magnet improves antitumor effect of vinblastine and the suppression of metastasis.** *Cancer Sci* 2009, **100:**1537–1543.
16. Wang L, Neoh KG, Kang ET, Shuter B: **Multifunctional polyglycerol-grafted Fe_3O_4@SiO_2 nanoparticles for targeting ovarian cancer cells.** *Biomaterials* 2011, **32:**2166–2173.
17. Wang F, Chen XL, Zhao ZX, Tang SH, Huang XQ, Lin CH, Cai CB, Zheng NF, Mater J: **Synthesis of magnetic, fluorescent and mesoporous core-shell-structured nanoparticles for imaging, targeting and photodynamic therapy.** *J Mater Chem* 2011, **21:**11244–11252.
18. Lin YS, Haynes CL: **Synthesis and characterization of biocompatible and size-tunable multifunctional porous silica nanoparticles.** *Chem Mater* 2009, **21:**3979–3986.
19. Chen Y, Chen HR, Shi JL: **In vivo bio-safety evaluations and diagnostic/therapeutic applications of chemically designed mesoporous silica nanoparticles.** *Adv Mater* 2013, **25:**3144–3176.
20. Reddy LH, Arias JL, Nicolas J, Couvreur P: **Magnetic nanoparticles: design and characterization, toxicity and biocompatibility, pharmaceutical and biomedical applications.** *Chem Rev* 2012, **112:**5818–5878.

21. Kim J, Kim HS, Lee N, Kim T, Kim H, Yu T, Song IC, Moon WK, Hyeon T: **Multifunctional uniform nanoparticles composed of a magnetite nanocrystal core and a mesoporous silica shell for magnetic resonance and fluorescence imaging and for drug delivery.** *Angew Chem Int Ed* 2008, **47:**8438–8441.
22. Laudenslager MJ, Schiffman JD, Schauer CL: **Carboxymethyl chitosan as a matrix material for platinum, gold, and silver nanoparticles.** *Biomacromolecules* 2008, **9:**2682–2685.
23. Shi ZL, Neoh KG, Kang ET, Shuter B, Wang SC, Poh C, Wang W: **(Carboxymethyl)chitosan modified superparamagnetic iron oxide nanoparticles for magnetic resonance imaging of stem cells.** *ACS Appl Mater Interfaces* 2009, **1:**328–335.
24. Fan CX, Gao WH, Chen ZX, Fan HY, Li MY, Deng FJ, Chen ZL: **Tumor selectivity of stealth multi-functionalized superparamagnetic iron oxide nanoparticles.** *Int J Pharm* 2011, **404:**180–190.
25. Oh JM, Choi SJ, Lee GE, Han SH, Choy JH: **Inorganic drug-delivery nanovehicle conjugated with cancer-cell-specific ligand.** *Adv Funct Mater* 2009, **19:**1617–1624.
26. Santra S, Kaittanis C, Santiesteban OJ, Perez JM: **Cell-specific, activatable, and theranostic prodrug for dual-targeted cancer imaging and therapy.** *J Am Chem Soc* 2011, **133:**16680–16688.
27. Peng S, Wang C, Xie J, Sun SH: **Synthesis and stabilization of monodisperse Fe nanoparticles.** *J Am Chem Soc* 2006, **128:**10676–10677.
28. Yi DK, Lee SS, Papaefthymiou GC, Ying JY: **Nanoparticle architectures templated by SiO_2/Fe_2O_3 nanocomposites.** *Chem Mater* 2006, **18:**614–619.
29. Parveen S, Sahoo SK: **Evaluation of cytotoxicity and mechanism of apoptosis of doxorubicin using folate-decorated chitosan nanoparticles for targeted delivery to retinoblastoma.** *Cancer Nano* 2010, **1:**47–62.
30. Li JC, Zheng LF, Cai HD, Sun WJ, Shen MW, Zhang GX, Shi XY: **Polyethyleneimine-mediated synthesis of folic acid-targeted iron oxide nanoparticles for in vivo tumor MR imaging.** *Biomaterials* 2013, **34:**8382–8392.
31. Zhu YF, Fang Y, Kaskel S: **Folate-conjugated Fe_3O_4@SiO_2 hollow mesoporous spheres for targeted anticancer drug delivery.** *J Phys Chem C* 2010, **114:**16382–16388.
32. Wana A, Sun Y, Li HL: **Characterization of folate-graft-chitosan as a scaffold for nitric oxide release.** *Int J Biol Macromol* 2008, **43:**415–421.
33. Yang SJ, Lin FH, Tsai KC, Wei MF, Tsai HM, Wong JM, Shieh MJ: **Folic acid-conjugated chitosan nanoparticles enhanced protoporphyrin IX accumulation in colorectal cancer cells.** *Bioconjugate Chem* 2010, **21:**679–689.
34. Veiseh O, Sun C, Kohler GNJ, Gabikian P, Lee D, Bhattarai N, Ellenbogen R, Sze R, Hallahan A, Olson J, Zhang MQ: **Optical and MRI multifunctional nanoprobe for targeting gliomas.** *Nano Lett* 2005, **5:**1003–1008.
35. Wei W, Zhang Q, Zheng XW: **Synthesis of chitosan/Fe_3O_4/SiO_2 nanocomposites and investigation into their catalysis properties.** *Acta Chim Sinica* 2013, **71:**387–391.
36. Shen JM, Guan XM, Liu XY, Lan JF, Cheng T, Zhang HX: **Luminescent/magnetic hybrid nanoparticles with folate-conjugated peptide composites for tumor-targeted drug delivery.** *Bioconjugate Chem* 2012, **23:**1010–1021.
37. Bhattacharya D, Das M, Mishra D, Banerjee I, Sahu SK, Maiti TK, Pramanik P: **Folate receptor targeted, carboxymethyl chitosan functionalized iron oxide nanoparticles: a novel ultradispersed nanoconjugates for bimodal imaging.** *Nanoscale* 2011, **3:**1653–1662.
38. Lin YS, Haynes CL: **Impacts of mesoporous silica nanoparticle size, pore ordering, and pore integrity on hemolytic activity.** *J Am Chem Soc* 2010, **132:**4834–4842.

doi:10.1186/1556-276X-9-146
Cite this article as: Li *et al.*: Carboxymethyl chitosan-folic acid-conjugated Fe_3O_4@SiO_2 as a safe and targeting antitumor nanovehicle *in vitro*. *Nanoscale Research Letters* 2014 **9**:146.